Chapter 1
Micro-Structuring and Ferroelectric Domain Engineering of Single Crystal Lithium Niobate

S. Mailis, C.L. Sones, and R.W. Eason

1.1 Introduction

The ability to microstructure specific materials is always associated with the ability to selectively remove material over small scale-lengths. Localized etching whether it is chemical or physical, wet or dry, parallel or sequential is central to every modern microstructuring method. For example a beam of accelerated ions is scanned on the surface of interest removing material along its trajectory. Alternatively the surface is prepared/treated in a manner that changes its "quality" locally making it more susceptible or more resistive to a particular etching agent. The whole surface is subsequently exposed to the etching agent which can be a uniform accelerated ion beam, a laser beam or an acid. The etching agent preferentially attacks the pre-treated (or the untreated) portion of the surface removing material.

In the case of silicon crystals there are anisotropic chemical etching agents which attack preferentially specific crystallographic planes [1]. Etching using these agents produces 3D structures while selective oxidization followed by HF etching is used for undercutting and slicing. It is fair to say that micro-structuring in the case of silicon crystals has managed to revolutionize silicon based devices and to produce a novel class of technology i.e. Micro-Electro-Mechanical-Systems (MEMS) [2–4].

Lithium niobate is a well established material which is widely used in photonics and, similar to silicon, excellent quality material is available at low cost. As in the case of silicon, microstructuring of lithium niobate is also expected to add functionality and value to the material by both improving the performance of existing devices and also by creating new ones.

In the rest of the chapter we will demonstrate how ferroelectric domain engineering, achieved mainly by the application of an external electric field at room temperature [5, 6], can be combined with subsequent chemical etching to provide a powerful method for the microstructuring of lithium niobate.

S. Mailis (✉) · C.L. Sones · R.W. Eason
Optoelectronics Research Centre, University of Southampton, Southampton SO17 1BJ, UK
e-mail: sm@orc.soton.ac.uk

P. Ferraro et al. (eds.), *Ferroelectric Crystals for Photonic Applications*,
Springer Series in Materials Science 91, DOI 10.1007/978-3-642-41086-4_1,

However, before embarking into the description of differential chemical etching of domain-engineered structures we present other methods that have been used for the microstructuring of lithium niobate. The methods listed here have been developed for the microelectronics industry hence they are considered standard and are very well characterized.

1.2 Other Methods

A high-precision method for micro-etching is *electron beam milling*. In this method a beam of accelerated electrons is scanned across the sample to remove material from the surface. The resolution of the features which can be fabricated with this method can be very high and is comparable to the effective wavelength of the accelerated electrons however, although very precise, this method is slow when etching of large surfaces is required. Electron beam milling has been used not only for the fabrication of microstructures in lithium niobate [7] but also for ferroelectric domain inversion [8, 9].

A method similar to the electron beam milling is *ion beam milling* where accelerated ions are used instead of electrons to selectively remove material. Focussed ion beam milling has been used successfully for the fabrication of ultra fine photonic structures in lithium niobate [10, 11]. However, this method is again limited due to its sequential nature and can only be sensibly applied for small areas ($\leq$1 mm). In another arrangement a broad beam of accelerated argon ions is used to bombard large sample areas that carry photolithographic patterning. Surface relief patterns are produced as the argon ions etch preferentially the parts of the material that are not covered by the photoresist. This arrangement is more suitable for the fabrication of extended structures across full wafers but its resolution is limited to the resolution of the photolithography.

Reactive ion etching is used in conjunction with photolithography, as in the case of ion beam milling to produce surface relief structures. In this method etching is aided by reaction of the ion species with the material to be etched. This method has been used for the fabrication of ridge waveguides and other photonic structures in lithium niobate [12–14].

Laser ablation or laser sputtering is a straightforward method whereby a highly absorbed (usually UV) laser beam is used to induce explosive evaporation of material from the surface. Part of the absorbed energy becomes kinetic energy of the part of the removed material which is ejected form the illuminated area. Etching of small features (suitable for photonic applications) can be achieved either by simply focusing of the laser beam, by using an absorption mask either in contact or projection mode and finally by interference [15–17]. Laser ablation is a "dirty" method because usually there is a large quantity of debris caused by re-deposition of the ejected material around the etched feature. However, subsequent cleaning or even brief wet etching can significantly improve the quality of the features.

Finally *wet etching* is another microstructuring method (one that is discussed at length here) whereby use of chemical reagents which interact with the surface

results in material removal at the interface between the surface and the reagent. Spatially selective etching is achieved by covering the surface with an inert film that inhibits the contact of the acid with that particular part of the surface or, as in the case of lithium niobate, by modifying the "type" of the interacting surface by inversion of the ferroelectric domain orientation.

1.3 Differential Chemical Etching

1.3.1 z-Faces

Chemical etching is often used for cleaning, polishing and purification of optical surfaces. For this purpose a number of potential etch/polish chemical reagents were examined in the comprehensive work by Nassau et al. [18] in a variety of experimental conditions to assess their ability to polish/etch lithium niobate single crystal surfaces. This study showed that certain chemical reagents were able to induce an optical contrast between opposite ferroelectric domains thus making them visible.

More specifically it was observed that optical contrast appeared between opposite ferroelectric domains on the z faces of the crystal after 15 sec to 60 sec immersion in molten KOH or 15 minutes in a hot (50 °C) mixture of H_2O_2 and NaOH. However, the highest contrast between opposite ferroelectric domains was observed for the HF:2HNO_3 mixture ratio [18]. This particular mixture of acids attacks preferentially the $-z$ face (defined as the z face that becomes negative upon cooling of the crystal [19]) removing material from the surface while the opposite $+z$ face remains unaffected. As a result of this effect any ferroelectric domain pattern will be transformed into a surface relief pattern after etching.

Brief (few minutes) etching in a mixture of HF and HNO_3 acid mixtures is today common practice for the quality assessment of nonlinear optical periodically poled lithium niobate (PPLN) devices. The relief pattern which is the result of differential etching corresponds precisely to the inverted ferroelectric domain shape and increases dramatically the optical contrast of the domain walls. Although destructive, it is still a very popular method for visualization of inverted domains in lithium niobate because it can show structural details of the domain boundary down to the nm scale.

Figure 1.1 shows two scanning electron microscopy (SEM) images corresponding to the opposite faces of a briefly (10 min) etched, hexagonally poled lithium niobate crystal (HexLN) which is a z-cut crystal that carries hexagonally shaped inverted ferroelectric domains arranged in a 2D hexagonal lattice [20]. The recessed hexagons shown in Fig. 1.1(a) correspond to the $-z$ face of the inverted ferroelectric domains that have been attacked preferentially by the acid. The surrounding area corresponds to a $+z$ face and hence stays unaffected, resulting in the observed difference in height. As the polarity of the domain terminating surfaces is inverted on the opposite face of the sample the surface topography after etching is complementary to that of Fig. 1.1(a), and appears as an inverted pattern as shown in Fig. 1.1(b).

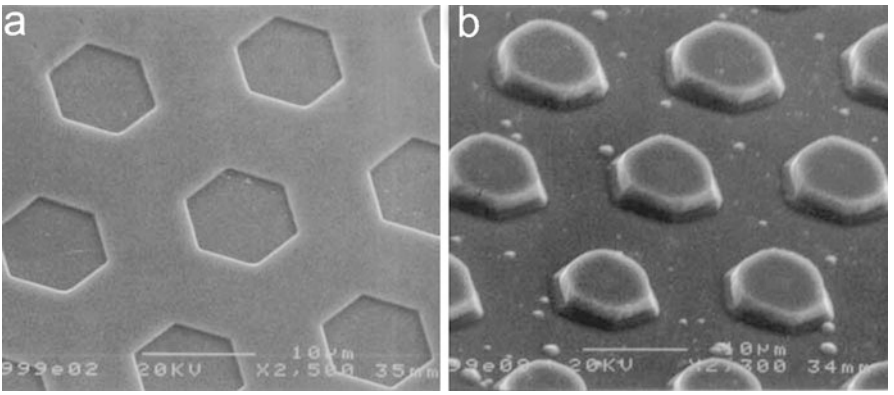

Fig. 1.1 SEM of briefly (10 min) etched hexagonally poled lithium niobate crystal: (**a**) $-z$ face terminating hexagonal domains, (**b**) $+z$ face terminating hexagonal domains

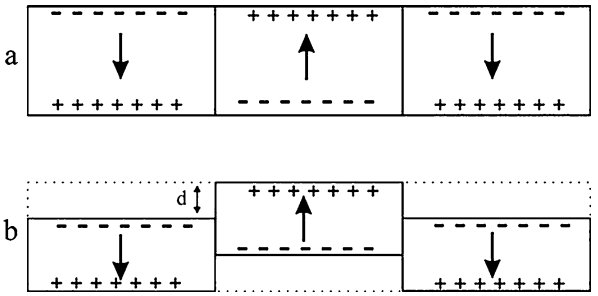

Fig. 1.2 Schematic showing the dependence of the preferential acid attack on the polarity of the electric dipole terminating surface, as indicated by the *arrows*

Etch-Rates

In the context of fabricating physical (high aspect ratio) structures it is necessary to etch the crystal for longer time (few hours to a few days depending on etching temperature and target etch depth) and to be able to predict the depth of the etching accurately. Hence, for any practical application it is useful to know the etching characteristics (etch-rate and quality) prolonged etching performed under different conditions. In a simple experiment, domain-engineered samples are etched for a fixed duration (15 hrs) at a temperature of 60 °C in HF:xHNO$_3$ ratios where $x = 0$, 1, 2, 4. The initial concentrations of the electronic grade HF and HNO$_3$ as supplied were 48 % and 78 % respectively. Upon etching a difference in height is produced between anti-parallel domain termination areas on opposite z faces of the crystal because the $-z$ termination area is preferentially attacked by the acids. A schematic of the etch behaviour of the opposite domain surfaces is shown in Fig. 1.2 where arrows are used to indicate the direction of the permanent dipole. The sign of the charge that appears on the polar surfaces upon cooling of the crystal is also indicated in the schematic.

The difference in step height "d" along a single interface between opposite domains corresponds to the etch depth of the $-z$ face. The topography of the interface

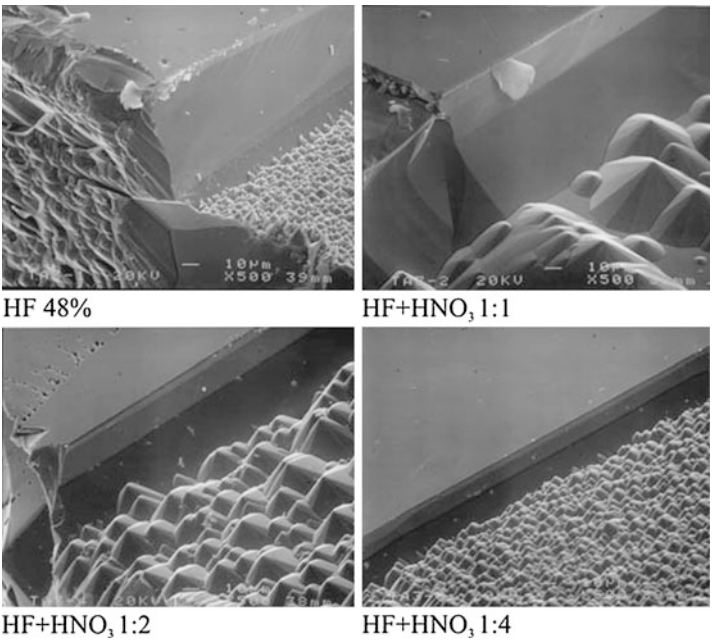

Fig. 1.3 SEM scans of the boundary between two inverted domains after etching for 15 hours in different HF:HNO_3 acid mixture ratios. The magnification is the same in all the scans

Table 1.1 Etch-rate as a function of HF:HNO_3 ratio at 60 °C

HF:HNO_3	% HF in mixture	d (μm)	Etch-rate (μm/hr)
0:1	0	0	0
1:4	9.6	26.2 ± 0.7	1.7
1:2	16	48.3 ± 2.4	3.2
1:1	24	70.9 ± 1.8	4.7
1:0	48	81.9 ± 20.0	5.5

between opposite domains etched with mixtures of different HF and HNO_3 acid ratios at 60 °C for 15 hrs is shown in the SEM images of Fig. 1.3. The step which is formed at the interface between opposite domains was measured using an α-step surface profiler, and the deduced etch-rates values (in μm/hr) as a function of the HF:HNO_3 mixture ratio are presented in Table 1.1.

The plot of the etch-rate as a function of the HF concentration in HF:HNO_3 mixture is shown in Fig. 1.4 where the ratio of acids is indicated in brackets next to the data points. The etch-rate increases with increasing temperature of the acid following an Arrhenius law [21].

This experiment concludes that pure HF provides the fastest etching-rate for the $-z$ face of lithium niobate and also that pure HNO_3 acid is not capable of etching

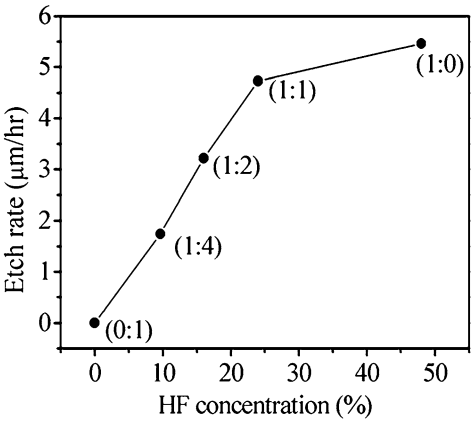

Fig. 1.4 Etch-rate at 60 °C for various ratios of HF and HNO_3 acids. The *horizontal axis* shows the concentration of HF in the mixture while the *brackets* next to the experimental points indicate the acid ratio (HF:HNO_3)

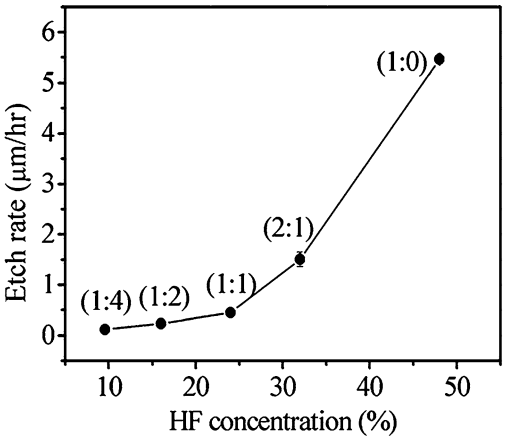

Fig. 1.5 Etch-rate of the $-z$ face at 60 °C as a function of the concentration of HF acid. The *horizontal axis* shows the concentration of HF in the mixture while the *brackets* next to the experimental points indicate the acid ratio (HF:HNO_3)

the crystal, at least by any measurable amount, for the etching conditions employed in the experiment. In another experiment the HNO_3 acid in the mixture is substituted with water and again a domain engineered sample was etched for the same duration and temperature with different concentrations of HF. The etch-rates of the $-z$ face were deduced and are shown in the plot of Fig. 1.5 as a function of the HF concentration in the etching solution.

It can be observed in this plot that the etch-rates were slower for water diluted HF which indicates that HNO_3 does play an auxiliary role in the etch process. More details about the chemistry of differential etching of lithium niobate in HF can be found in [22, 23].

Prolonged etching of the $-z$ face of the crystal affects the quality of the etched surface usually resulting in significant surface roughness, which is not desirable of course in any micro-fabrication processes. However, the quality of the etched surface after prolonged etching can be controlled to some extent by the ratio of HF and HNO_3 mixture. Figure 1.6 shows a sequence of SEM images corresponding to the

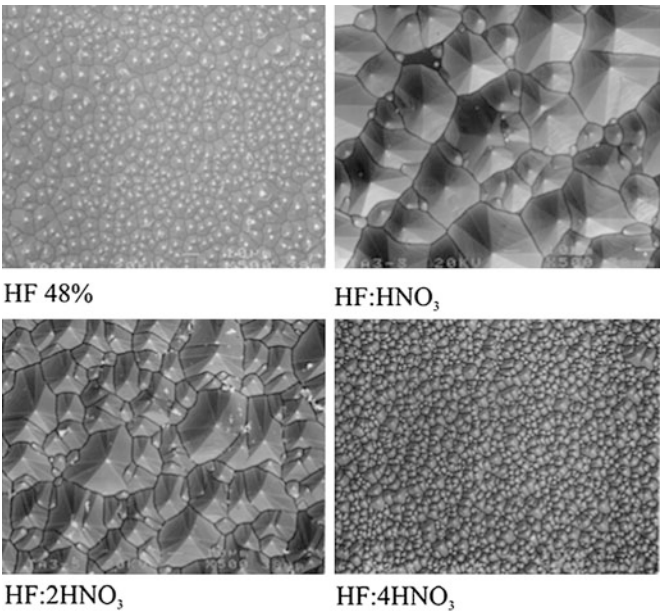

Fig. 1.6 SEM scan of the $-z$ face after 15 hours of etching at 60 °C with different HF:HNO_3 ratios. The magnification is the same in all four scans

crystal surface after etching for the same duration and temperature but with different acid mixture ratios. In order to exclude the possibility of material quality variation, the samples used in this experiment came from the same wafer. It is obvious that the HF:HNO_3 mixture ratio can dramatically change the surface topography and furthermore, it seems that pure HF (48 %) etching not only is faster but gives the best etched surface quality.

There are however several indications that the chemical etching induced surface roughness can be further controlled e.g. by changing the temperature of the process or by other pre-treatment of the surface such as UV illumination.

1.3.2 y-Faces

Careful observation of etched single inverted ferroelectric domains shows that the original shape of the inverted domain is not preserved during the etch process. This is indicative of simultaneous etching of more than one crystal planes/surfaces. To demonstrate this more clearly we have etched a sample similar to the one shown in Fig. 1.1 for 24 hrs. The initial inverted domain distribution consists of hexagonally shaped domains arranged in a hexagonal close packed 2D lattice. The result of the prolonged etching is shown in Fig. 1.7. These SEM images correspond to the two opposite faces of the sample show upstanding features (Fig. 1.7(a)) and cavities (Fig. 1.7(b)) arranged in the original 2D hexagonal lattice.

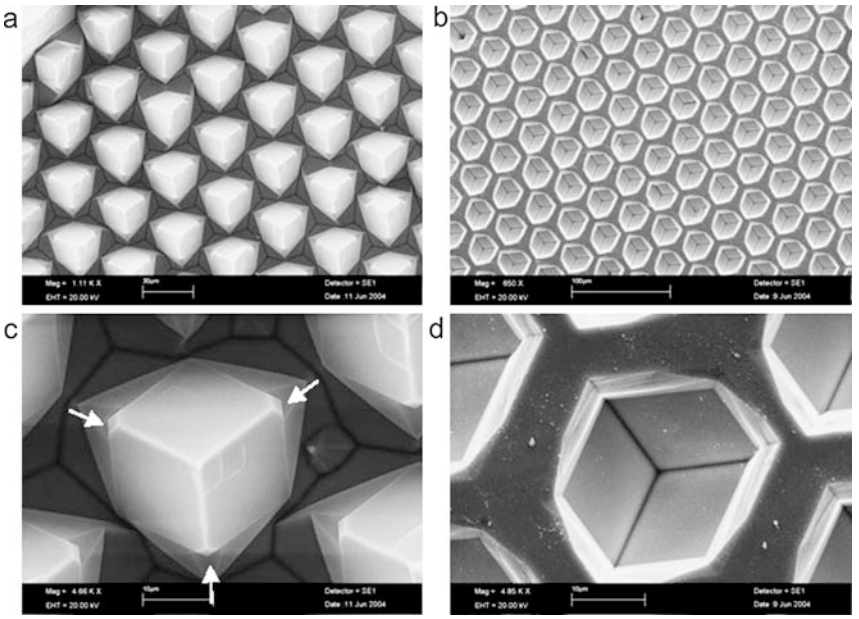

Fig. 1.7 SEM scans of opposite faces of a prolonged HF etched HexLN crystal. (**a**) Pyramids corresponding to $+z$ terminating domains, (**b**) cavities corresponding to $-z$ face terminating domains, (**c**), (**d**) higher magnification scans of (**a**) and (**b**) respectively

However, the cross section of these features transforms from hexagonal at the base to triangular at the top and finally degenerates to a point at the very top as the faces of the triangle merge. This is more obvious in the higher magnification images shown in Fig. 1.7(c), (d).

This transformation of the shape of the etched feature can be attributed to a lateral etching taking place simultaneously with the vertical etching process (along the z direction). Since the lateral etching is not pronounced after brief etching we can conclude that it is much slower than the primary etching along the z direction. Lateral etching is also not uniform because if it was, the cross section of the etched structures would tend to become circular rather than triangular. From the symmetry of the resulting pyramidal structures we can deduce that the lateral etching occurs between opposite y-face pairs and the etch-rate depends on the "polarity" of the y-face.

As shown in Fig. 1.8, the three indistinguishable y-directions in lithium niobate single crystals, contained within the three mirror planes, and normal to the z axis, clearly explains the transformation from hexagonal to a triangular shape. The schematic illustrates the shape transformation of a hexagonal domain as a result of lateral y-face etching. One can notice that the apices of the initial hexagonal domain that correspond to $+y$ faces stay pinned in the schematic. Further etching reduces the size of the hexagon hence the apices start to move until the triangular shape degenerates to a single point (not shown in the schematic).

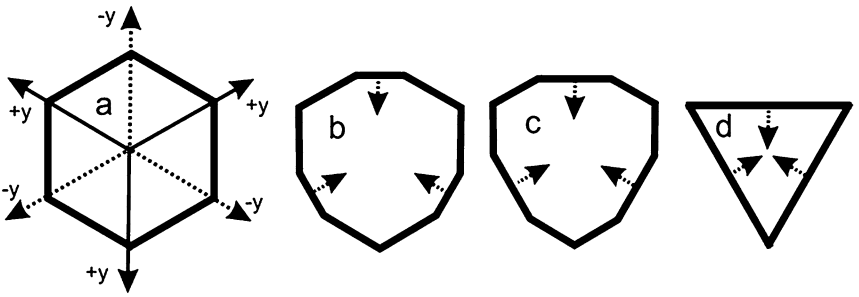

Fig. 1.8 Schematic illustrating the shape transformation of the top surface of an isolated hexagonal domain due to differential y-face etching. From left to right: (**a**) initial shape of the etched domain, the *axes* indicate the three y symmetry directions and their polarity, (**b**) and (**c**) intermediate stages where the *arrows* show the etch directions, (**d**) the final triangular shape

This shape transformation is common for both faces of the domain and only the etch direction is different. The etching process of opposite y-faces unlike the differential etching between opposite z-faces, affects both faces. This can be observed near the base of the triangular pyramid in the areas which are indicated by the arrows in Fig. 1.7(c). In these areas the tips of the triangular cross section (which correspond to the $+y$-face that etches slower) are flattened as a result of etching.

The direction of the y-axes is inverted during ferroelectric domain inversion [24] hence, the depth profile of inverted ferroelectric domains can be visualized by etching of the y-face [25]. Finally, there is no observation in the prolonged etching of inverted domains structures to suggest that the x-faces of the crystal etch at all in HF and HNO_3 mixtures and if there is any x-face etching at all the rate should be remarkably slow. At this point it is worth mentioning that the pyramids which are produced by etching of individual hexagonal domains like the ones shown in Fig. 1.7 terminate in ultra-sharp tips which could be used in scanning probe microscopy. A side view of a pyramid array and a high magnification of the ultra-sharp tip are shown in the SEM images of Fig. 1.9.

1.3.3 Microstructures

The next step now will be to show how this very important feature i.e. differential etching between opposite domains can be used to fabricate 2D and 3D microstructures in lithium niobate single crystals.

Direct Etching of Domain-Inverted Crystals

From the previous discussion it is clear that direct chemical etching of a ferroelectric domain distribution results in the generation of a surface relief pattern. Prolonged

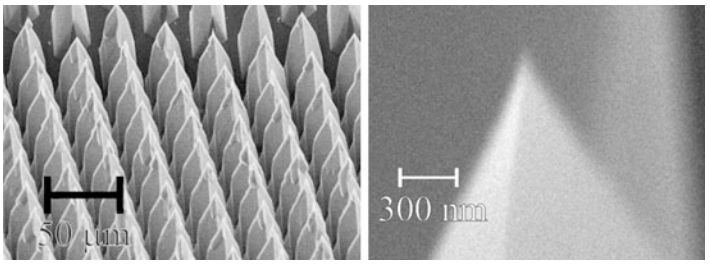

Fig. 1.9 SEM images of: (*left*) side view of an array of pyramids and (*right*) high magnification side-view of the terminating tip

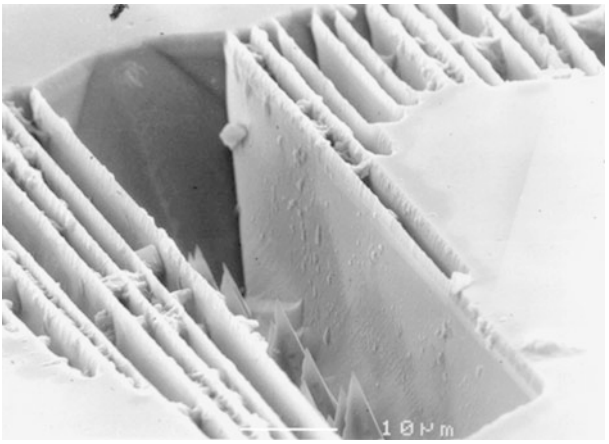

Fig. 1.10 SEM scan of a high aspect ratio structure fabricated by long etching of a periodically poled lithium niobate crystal

etching can indeed result in very high aspect ratio structures an example of which is illustrated in Fig. 1.10 where an SEM image of a periodically poled crystal which has been etched for a few hours is shown. The inverted domain slabs in this structure have a width of approximately 2 μm and a depth of ∼20 μm. The quality and depth of the vertical wall which corresponds to the inverted domain sheet can be clearly observed through the gap left by missing PPLN. There are numerous applications that can benefit from structures like these.

Figure 1.11 shows SEM images of a set of waveguide ridges fabricated by the chemical HF etching of a set of stripe inverted domains. The vertical confinement of light is achieved by subsequent titanium indiffusion [26]. Waveguiding takes place in the top ∼2–3 μm of the ridge which is away from the rough surface of the etched $-z$ face as shown in Fig. 1.11(b). The side wall of the ridge structure is very smooth, free from any roughness that could induce optical loss.

Waveguides like the ones shown in Fig. 1.11 have been subsequently periodically poled and used to demonstrate nonlinear second harmonic generation [29].

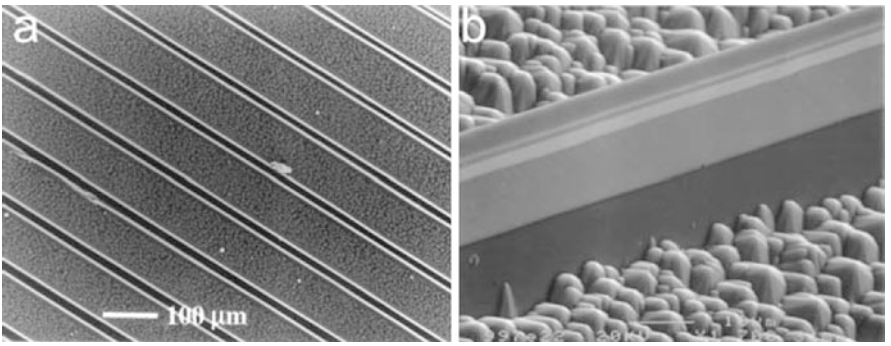

Fig. 1.11 (**a**) set of ridge waveguides; (**b**) high magnification side view of a single ridge waveguide

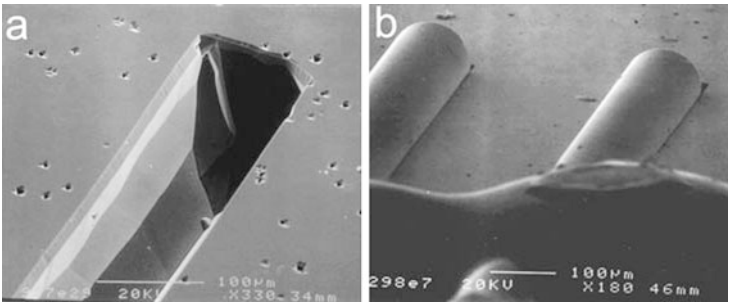

Fig. 1.12 (**a**) SEM image of a fiber alignment groove; (**b**) standard telecom fibers mounted into a pair of alignment grooves

Etched cavities can also be used for the precise alignment of optical components on a photonic chip. Shown in the SEM image of Fig. 1.12(a) is a set of etched cavities which are used for the mounting of two optical fibres onto a common substrate. This arrangement could be used for pigtailing of a photonic device pre- or post-fabricated on the substrate.

Other applications could include surface structuring for impedance matching in fast optical switches and acousto-optic waveguides. Additionally if the ferroelectric domain distributions become comparable to the optical wavelength of a guided wave in the crystal then etched periodic poled structures can be used as Bragg gratings [27] or photonic band-gaps for 2D structures [28].

Complex 3D Structures

Fabrication of 3D structures, especially free standing structures, involves a substantial complication as it is necessary to undercut (etch below) an existing structure, a task which cannot be achieved merely by domain engineering and etching.

One way to fabricate such structures is by employing the method of contact bonding [29–32]. This method relies on the Van Der Waals forces between two ultra-clean flat surfaces to maintain contact between them when brought to close proximity and is used routinely in the microelectronics industry.

This approach for fabrication of complex structures will be illustrated by following the steps for the fabrication of a set of free standing structure cantilevers which is a typical MEMS structure. For this purpose we will use an already processed substrate which carries all the undercut sections. This substrate is subsequently bonded to a second, structure-carrying, substrate forming a composite which can be further processed (polished, etched) as a whole.

The fabrication steps of the two separate substrates and the composite are outlined in the schematic which is shown in Fig. 1.13. The substrate shown on the left in the schematic is the one carrying the cantilever structures while the substrate on the right will form the basis of the structure.

In steps 1–3, as shown in the schematic, the two substrates are domain engineered in order to encode, in domain inverted patterns, the desired physical structures to be revealed after etching. The substrate on the left hand side of the schematic carries the cantilever structures while the substrate on the right hand side carries a large domain inverted square that provides the undercut section that allows the cantilevers to be free standing. The areas appearing grey in the schematic correspond to $-z$ face therefore material can be removed from this part of the surface by chemical HF etching.

In step 5 the composite is polished in order to reduce the thickness of the cantilever structure-carrying side. In this step the thickness of the cantilevers is defined and finally in the final step 6 the composite is chemically etched in HF to reveal the free standing cantilevers.

An example of the finished structure is shown in the SEM images of Fig. 1.14. The SEM image on the left shows the tip of the cantilever while the image on the right shows the point of support. The structure shown in Fig. 1.14 is $\sim$1 mm long, and has a top surface width of $\sim$50 μm and a height of $\sim$100 μm.

The cross-section of the cantilever however is not square because it is subject to lateral etching. In the image shown in Fig. 1.15 focussed gallium ions were used to cut off a part of the tip of the cantilever beam revealing its cross section which shows significant back etching as this particular sample has been over-etched.

Longer etching leads to more severe deformation of the original structure where in extreme cases the single cantilever can split into two beams with a common support point forming a structure that looks very much like a tuning fork.

The image shown in Fig. 1.16, taken using an optical microscope, shows that it is possible to focus through the free-standing beam. This indicates that the surfaces of the cantilever maintain their good optical quality during the fabrication process which is very important for any optical waveguide arrangement superimposed onto the physical structure.

Tuneability is one unique feature of lithium niobate crystals that makes this material particularly attractive for use in optical devices. The optical and mechanical properties of the crystal can be modified by a small amount by (among others) the

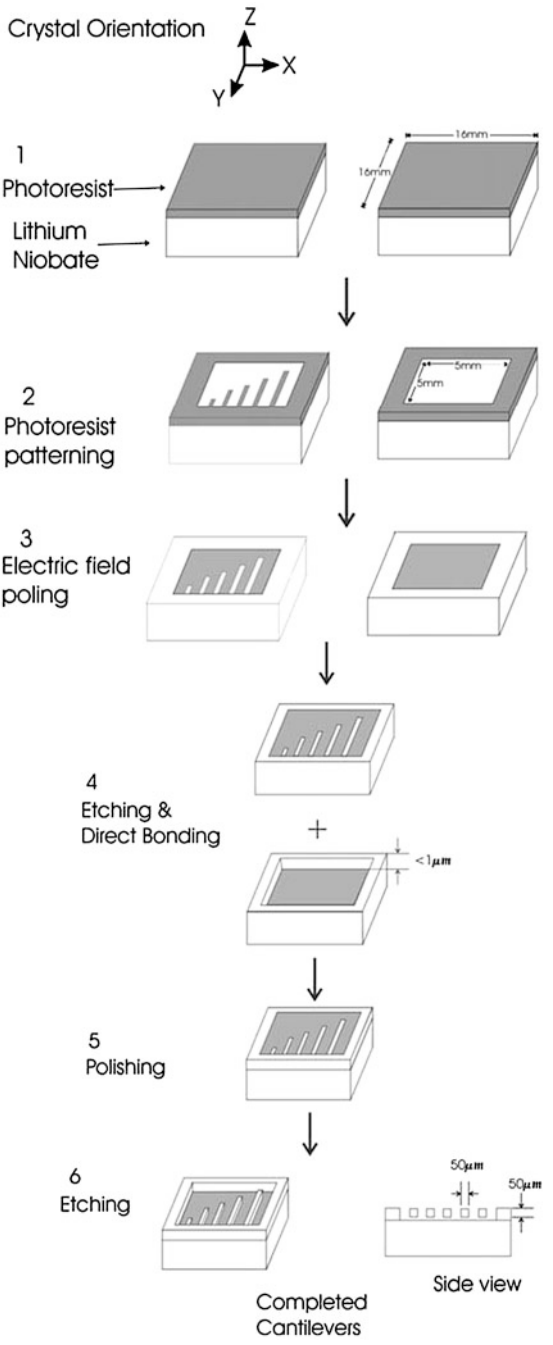

Fig. 1.13 Schematic illustrating the steps for the fabrication of free standing single crystal cantilevers

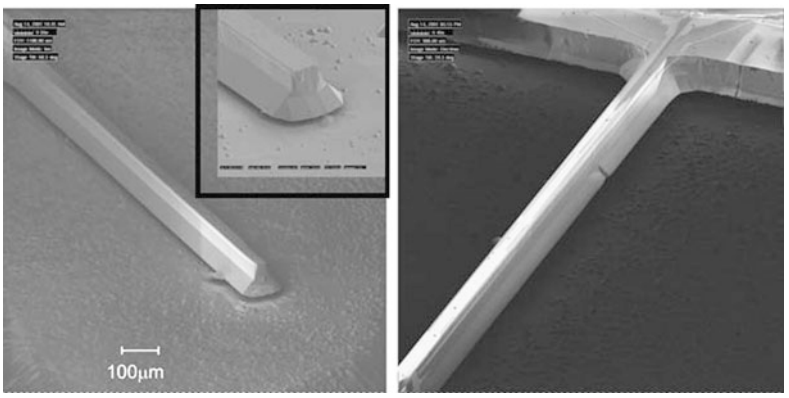

Fig. 1.14 SEM scans of a single crystal lithium niobate micro cantilever. *Left*: the tip of the structure, *right*: the support point, *inset*: high magnification image of the cantilever tip

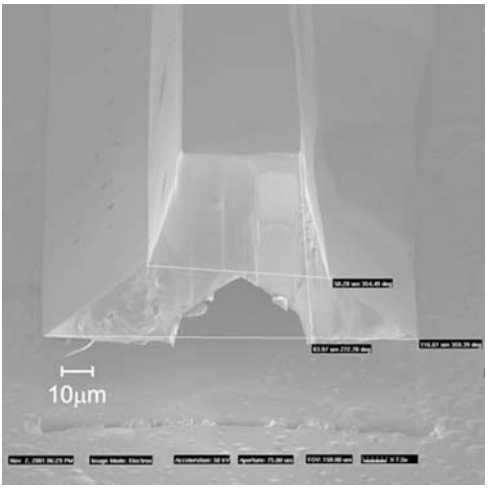

Fig. 1.15 Cross-section of a lithium niobate micro-cantilever

application of an electric field. Hence, any device will need to be equipped with electrodes that deliver the appropriate voltages locally. One way to deposit metals with precision is by using a focused ion beam to break down metalorganic precursors in the vicinity of the surface.

Although time consuming (depending on the size of the electrode) this is a very precise and straightforward method for fabricating electrical contacts. Deposition of tungsten (W) electrodes along the sides of a single crystal pyramid and a cantilever beam is shown in the SEM images of Fig. 1.17.

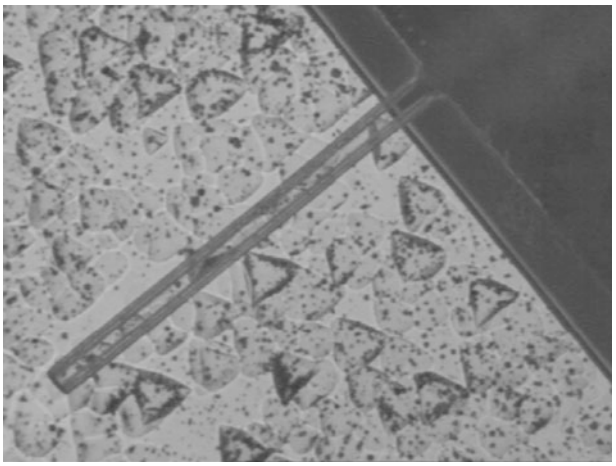

Fig. 1.16 Optical microscope image of a free-standing cantilever. The rougher undercut substrate is visible through the bulk of the cantilever

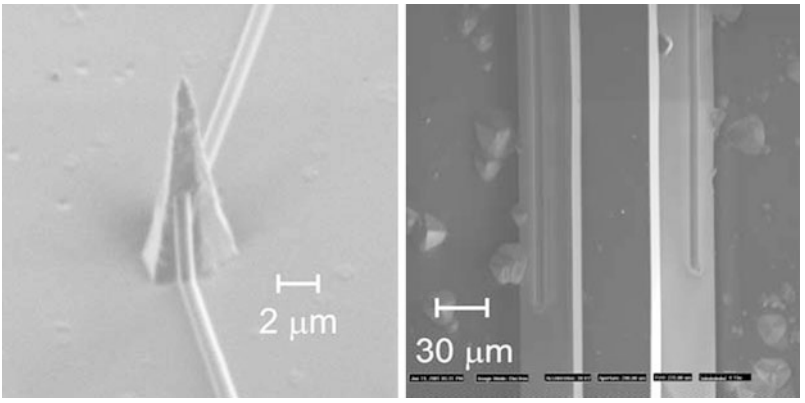

Fig. 1.17 Tungsten electrodes deposited by FIB induced CVD along the side surface of a single crystal tip (*left*) and a cantilever beam (*right*)

1.4 Summary and Future Work

Differential chemical etching between opposite z faces of lithium niobate crystals has been known to researchers since the discovery and initial experimental growth of crystals. While this effect has been extensively used for the assessment of the crystal quality in this chapter we have shown how differential etching between opposite z faces can be used for microstructuring of domain-engineered crystals. We have shown studies of the etch-rates under different conditions and discussed the simultaneous lateral differential etching between opposite y-faces and its impact on the topography of the resulting structures.

The better understanding of the differential etching process has helped to optimize it and furthermore to employ it in the fabrication of a variety of structures ranging from simple 2D surface structures to high aspect ratio 3D microstructures and finally, incorporation of the standard fabrication technique of contact bonding has enabled the realization of free standing structures such as a single crystal microcantilever. Structures which are fabricated using differential etching of ferroelectric domains benefit from the high optical quality of the etched facets which enables potential integration of optical structures onto the physical structures.

Finally, we have identified the method of chemical vapour deposition induced by FIB for the application of metal electrodes onto delicate micro-structures.

The micro-fabrication method that we have presented here however does not represent a panacea. There are still a number of processing issues that have to be addressed, especially if there is a scope for industrial scale fabrication. In reality it is necessary to consider all microfabrication methods and apply the suitable one for different intended structures. The message that we would like to emphasize with this chapter however is that there is indeed an extensive toolbox available for the microfabrication of lithium niobate and that it is feasible to fabricate complex structures thus expanding the application range, increasing the degree of integration and adding value to this very important nonlinear optical ferroelectric material.

References

1. K.E. Petersen, Proc. IEEE **70**, 420–456 (1982)
2. W.P. Eaton, J.H. Smith, Smart Mater. Struct. **6**, 530–539 (1997)
3. T. Frank, J. Micromech. Microeng. **8**, 114–118 (1998)
4. M. Koch, D. Chatelain, A.G.R. Evans, A. Brunnschweiler, J. Micromech. Microeng. **8**, 123–126 (1998)
5. M. Yamada, N. Nada, M. Saitoh, K. Watanabe, Appl. Phys. Lett. **62**, 435 (1993)
6. J. Webjorn, V. Pruneri, St.P.J. Russell, J.R.M. Barr, D.C. Hanna, Electron. Lett. **30**, 894 (1994)
7. C. Restoin, S. Massy, C. Darraud-Taupiac, A. Barthelemy, Opt. Mater. **22**, 193 (2003)
8. C. Restoin, C. Darraud-Taupiac, J.L. Decossas, J.C. Vareille, J. Hauden, Mater. Sci. Semicond. Process. **3**, 405–407 (2000)
9. A.C.G. Nutt, V. Gopalan, M.C. Gupta, Appl. Phys. Lett. **60**, 2828 (1992)
10. S.Z. Yin, Microw. Opt. Technol. Lett. **22**, 396 (1999)
11. F. Lacour, N. Courjal, M.P. Bernal, A. Sabac, C. Bainier, M. Spajer, Opt. Mater. **27**, 1421 (2005)
12. H. Hu, A.P. Milenin, R.B. Wehrspohn, H. Hermann, W. Sohler, J. Vac. Sci. Technol. A **24**, 1012–1015 (2006)
13. V. Foglietti, E. Cianci, D. Pezzeta, C. Sibilia, M. Marangoni, R. Osellame, R. Ramponi, Microelectron. Eng. **67–68**, 742 (2003)
14. W.S. Yang, H.Y. Lee, W.K. Kim, D.H. Yoon, Opt. Mater. **27**, 1642–1646 (2005)
15. H.W. Chong, A. Mitchell, J.P. Hayes, M.W. Austin, Appl. Surf. Sci. **201**(1–4), 196–203 (2002)
16. L. Gui, B.X. Xu, T.C. Chong, IEEE Photonics Technol. Lett. **16**, 1337–1339 (2004)
17. S. Mailis, G.W. Ross, L. Reekie, J.A. Abernethy, R.W. Eason, Electron. Lett. **36**, 1801–1803 (2000)
18. K. Nassau, H.J. Levinstein, G.M. Loiacono, J. Phys. Chem. Solids **27**, 983 (1966)
19. R.S. Weis, T.K. Gaylord, Appl. Phys. A **37**, 191–203 (1985)

20. N.G.R. Broderick, G.W. Ross, H.L. Offerhaus, D.J. Richardson, D.C. Hanna, Phys. Rev. Lett. **84**, 4345 (2000)
21. I.E. Barry, G.W. Ross, P.G.R. Smith, R.W. Eason, G. Cook, Mater. Lett. **37**, 246 (1998)
22. C.L. Sones, S. Mailis, W.S. Brocklesby, R.W. Eason, J.R. Owen, J. Mater. Chem. **12**, 295 (2002)
23. D. Xue, K. Kitamura, Ferroelectrics **29**, 89–93 (2002) (Letters section)
24. T.J. Sono, J.G. Scott, C.L. Sones, C.E. Valdivia, S. Mailis, R.W. Eason, J.G. Frey, L. Danos, Phys. Rev. B **74**, 205424 (2006)
25. N. Niizeki, T. Yamada, H. Toyoda, Jpn. J. Appl. Phys. **6**(3), 318–326 (1967)
26. I.E. Barry, G.W. Ross, P.G.R. Smith, R.W. Eason, Appl. Phys. Lett. **74**, 1487 (1999)
27. A.C. Busacca, C.L. Sones, V. Apostolopoulos, R.W. Eason, S. Mailis, Appl. Phys. Lett. **81**, 4946 (2002)
28. S. Grilli, P. Ferraro, L. Sansone, M. Paturzo, S. De Nicola, G. Plerattini, P. De Natale, IEEE Photonics Technol. Lett. **18**, 541–543 (2006)
29. K. Mitane, U. Goselr, J. Electron. Mater. **21**, 669 (1992)
30. F. Gray, K. Hermansson, Appl. Phys. Lett. **71**, 3400 (1997)
31. K. Ljungberg, A. Soderbarg, Y. Backlund, Appl. Phys. Lett. **78**, 1035 (1993)
32. H. Himi, H. Matsui, S. Fujino, T. Hattori, Jpn. J. Appl. Phys. **33**, 6 (1994)

http://www.springer.com/978-3-642-41085-7

Ferroelectric Crystals for Photonic Applications
Including Nanoscale Fabrication and Characterization
Techniques
Ferraro, P.; Grilli, S.; De Natale, P. (Eds.)
2014, XXII, 493 p. 309 illus., 43 illus. in color., Hardcover
ISBN: 978-3-642-41085-7